Isı Bilimi ve Tekniği Dergisi, 34, 2, 49-60, 2014
J. of Thermal Science and Technology

ISSN 1300-3615

EXPERIMENTAL INVESTIGATION AND NUMERICAL MODELING OF THERMAL PERFORMANCE OF FIN-TUBE EVAPORATOR UNDER FROSTING CONDITIONS

Dilek Nur ÖZEN*, Kemal ALTINIŞIK, Kevser DINCER*** and Ali ATEŞ******
Necmettin Erbakan University, Faculty of Engineering and Architecture, Department of Mechanical Engineering, Meram, Konya, Turkey, *dnozen@konya.edu.tr
Selcuk University, Faculty of Engineering, Department of Mechanical Engineering, Selcuklu, Konya, Turkey, **kaltinisik@selcuk.edu.tr, ***kdincer@selcuk.edu.tr, ****aates@selcuk.edu.tr

(Geliş Tarihi: 13.05.2013 Kabul Tarihi: 26.08.2013)

Abstract: Formation of frost in a heat exchanger reduces air passage area and lowers the performance of the heat exchanger due to the insulation effects it possesses. In this study, the performance of finned tube evaporator at transient regime was investigated both experimentally and numerically. When the experimentally obtained values of the evaporator's the total conductivity (UA) are compared with those obtained from the numerical model, it is found that they are very close to one another. On the numerical model, the effects of inlet air temperature, relative humidity and air velocity on evaporator's total conductivity (UA), air side pressure drop (ΔP_a) and frost thickness (δ_{fst}), were respectively, studied. The results obtained from the numerical model show that ΔP_a and δ_{fst} values increase with increasing air temperature and relative humidity while decreasing UA values.
Keywords: Finned tube, evaporator, heat transfer, frosting, transient state

KARLANMA KOŞULLARI ALTINDA KANATLI BORU EVAPORATÖRÜNÜN ISIL PERFORMANSININ DENEYSEL İNCELENMESİ VE SAYISAL MODELLENMESİ

Özet: Soğutma sistemlerinin evaporatörlerinde kar oluşumu, kanatlar arasındaki hava geçiş alanını azaltır ve yüzey üzerindeki yalıtım etkisi nedeniyle, evaporatörün performansı düşer. Bu çalışmada bir kanatlı borulu evaporatörün geçici (transient) rejimdeki performansı deneysel ve sayısal olarak incelendi. Evaporatörün toplam ısıl geçirgenliği, deneysel veriler ve sayısal modelden elde edilen sonuçlarla karsılastırıldığında; degerlerin birbirine cok yakın olduğu görüldü. Sayısal modelde hava giriş sıcaklığının, bağıl nemin ve hava hızlarının; evaporatörün toplam ısıl geçirgenliğine (UA), hava tarafı basınç düşümüne (ΔP_a) ve kar kalınlığına (δ_{fst}) etkisi incelendi. Sayısal modelden elde edilen sonuçlardan, görüldüğü gibi, hava sıcaklığı ve bağıl nem arttıkça UA değeri azalmakta, ΔP_a ve δ_{fst} değerleri ise artmaktadır.
Anahtar kelimeler: kanatlı boru, evaparator, ısı transferi, karlanma, geçici rejim

NOMENCLATURE

A	area (m^2)
A	coefficient in linearised relationship between saturation enthalpy of air and temperature ($h_{sat;T}$=a.T+b=1.4204+10.205) (J kg^{-1} K^{-1})
B_0	boiling number
c_p	specific heat (J kg^{-1} K^{-1})
D	diffusivity of water vapor in air (m^2 s^{-1})
D_h	hydraulic diameter (m)
F	constant fanning factor
H	convection heat transfer coefficient ($Wm^{-2}K^{-1}$)
h_{fg}	enthalpy of evaporation (J kg^{-1})
h_{sb}	enthalpy of sublimation (J kg^{-1})
h_L	liquid to liquid convection heat transfer coefficient ($Wm^{-2}K^{-1}$)
h_{TP}	two phase heat transfer coefficient ($Wm^{-2}K^{-1}$)
h_r	local evaporation heat transfer coefficient ($Wm^{-2}K^{-1}$)
k	thermal conductivity ($Wm^{-1}K^{-1}$)
L_{fin}	length of the fin (m)
L	equivalent height of the fin (m)
Le	Lewis number
M_a	mass per meter of air (kg m^{-1})
M_r	mass per meter of refrigerant (kg m^{-1})
M	mass (kg)
$\dot{m}$	mass flow rate (kg s^{-1})
m_w	mass flow from tube wall (kg)
m''_δ	amount of water vapor increasing frost thickness (kg $s^{-1}m^{-2}$)
m''_ρ	amount of water vapor increasing frost density (kg $s^{-1}m^{-2}$)
Nu	Nusselt number
Q	heat transfer (W)
q''	heat flux (W m^{-2})

P pressure (N m^{-2})
Pr Prandtl number
R radius (m)
Re Reynolds number
w_{fin} fin width (m)
t time (s)
T temperature (^oC)
U The overall heat transfer coefficient (W m^{-2} K^{-1})
$U_{a,f}$ total heat transfer coefficient from air to fin (W m^{-2} K^{-1})
$U_{a,t}$ total heat transfer coefficient from air to tube (W m^{-2} K^{-1})
U_m mass transfer coefficient of outside air (kg s^{-1} m^{-2})
$U_{a,r}$ coefficient of total heat transfer from air to refrigerator (W m^{-2} K^{-1})
UA The overall heat transfer coefficient of evaporator (W K^{-1})
X degree of dryness (kg kg^{-1})
x, y, z coordinate (m)

Greek letters

δ thickness (m)
ε_{fst} absorption coefficient
η efficiency
ρ density (kg m^{-3})
ω absolute humidity (kg kg^{-1})
Φ relative humidity (%)
Ψ_{bs} value in the bubble suppression regime
Ψ_{cb} value in pure convection boiling regime
Ψ_{nb} value in pure nucleus boiling regime

Subscripts

a air
fin fin
fst frost
I inside
O outside
R refrigerant
S surface
T total
T tube
Tab tab
V vapor
W wall

INTRODUCTION

Evaporators are devices that enable heat to be drawn from an area to be cooled through evaporation of a refrigerating fluid. In the no-frost refrigerators that work on the principle of air circulation cooling, finned tube evaporators are used. In such types of evaporators problems encountered as a result of low coefficient of heat convection on the air side are overcome by incorporating plate-shaped wings into the evaporators. This leads to an increase in the total heat transfer and the evaporator performance is improved too. In the domestic type refrigerators, there is usually formation of frost films on evaporator surfaces during the start up when the water vapor temperature is lower than the freezing temperature. If the frost surface temperature continues to remain under the freezing temperature, the frost will keep accumulating over the surface and acting as an insulating agent. This increases thermal resistance, lowers the heat amount the refrigerating fluid absorbs and increases energy consumption as a result of frost formation in between the fins. That's why it is quite important to consider frost formation during evaluation of performance of the energy efficient systems in the no-frost refrigerators.

In the existing literature, there are many numerical and experimental studies on performance of finned tube heat exchangers operating under frosting conditions. Some are briefly mentioned below. Kondepudi and O'Neal (1993) studied performance of finned-tube heat exchangers under frosting conditions: I. Simulation model. They reported that the results include frost accumulation and its effect on energy transfer in relation to varying humidities, fin densities and ambient conditions. Kondepudi and O'Neal (1993) investigated performance of finned-tube heat exchangers under frosting conditions: II. Comparison of experimental data with model. They noted that the data obtained from experiments were found to be within 15 20% of values predicted by the model.

Kondepudi and O'Neal (1989) presented effect of frost growth on the performance of louvered finned tube heat exchangers. They showed that higher air humidity, air face velocities and smaller fin spacing all led to increased frost growth, higher pressure drops and higher energy transfer coefficients. As frost accumulated on the heat exchanger, the overall energy transfer coefficient eventually dropped.

Yan et al. (2003) studied performance of finned tube heat exchangers operating under frosting conditions. They showed that the rate of pressure drop increases rapidly as the relative humidity increases. Tso et al. (2006) examined an improved model for predicting performance of finned tube heat exchanger under frosting condition, with frost thickness variation along fin. They noted that comparisons were made based on the frost mass accumulation, pressure drop across coil and energy transfer coefficient, and results were found to agree well with reported experimental results. Seker et al. (2004) provided frost formation on fin-and-tube heat exchangers. Part I-Modeling of frost formation on fin-and-tube heat exchangers. They reported that the model was partially based on utilizing empirical correlations for predicting frost thermal conductivity and the amount of water vapor increasing the frost density. Model results were compared with experimental results taken from literature and found to agree well in the applicable geometries. Hermes et al. (2009) advanced a theoretical and experimental investigation of the frost growth and densification on flat surfaces. They investigated experimentally in order to provide a physical basis for the development of a theoretical model to predict the variation of the frost layer thickness and mass with time. When they

compared with experimental data, the model predictions of the frost thickness as a function of time agreed to within ±10% error bands. Seker et al. (2004) presented some comparisons of the experimental data obtained with the analytical model presented in Part I of this paper. The comparisons were made in terms of airside pressure drop and the overall heat transfer coefficient. Lenic et al. (2009) made an analysis of heat and mass transfer during frost formation on a fin-and-tube heat exchanger has been presented. For calculation of an exchanged heat flux, a transient two-dimensional mathematical model of frost formation has been developed and numerically solved. The mathematical model and numerical procedure have been experimentally validated. They noted that the effectively exchanged heat flux significantly depends on operating conditions, such as air humidity and temperature, as well as the cooling cycle duration.

Getu and Bansal (2011) studied the fundamentals of experimental techniques for frost measurements and presents unique frost property correlations that are developed from experiments on a lab-scale flat-finned-tube heat exchanger. They reported that the newly developed correlations will be useful for better prediction and control of defrost periods and duration for medium-temperature (−10 °C) air coils.

Moallem et al. (2012) experimentally investigated the frost growth on louvered folded fins in microchannel heat exchangers when used in outdoor air-source heat pump systems. The effects of surface temperature, fin geometries, and air environmental conditions were studied. They showed that the frosting time and the frost growth rates depended mainly on the local fin surface temperature. Lower fin density was beneficial because it delayed the blockage of the air flow. The fin length and fin depth had minor effects on frosting performance. The air humidity had a fairly significant effect on rate of frost formation while air velocity seemed to have a small effect on the frost growth rate.

Wang et al. (2013) theoreticalyl study investigated the critical heat and mass transfer characteristics on a frosting tube. The parameters, Critical Frost Thickness (CFT) and Neutral Frost Thickness (NFT) were presented for the first time. They noted that the CFT and NFT were found to be more sensitive to the parameters of humidity , velocity and tube outside diameter.

In this study, performance of finned tube heat exchanger was investigated both experimentally and numerically. The experimental and numerical results were found to be compatible to one another (Situation 1). The UA, ΔP_a and frost thickness at different air conditions that were not conducted experimentally, were modeled numerically and presented in Situation 2.

There are a number of frost models in the literature. The distinctive feature of this study as opposed to the others in the literature is the formation of a frost model based on total heat transfer coefficient with the energy balance equations. The energy balance equations have been derived from the total heat transfer coefficients from air to tube surface, from air to fin surface and from air to the refrigerant. Comparisons between the results of this study and those of the other studies in the literature are given in Tables 3-5.

FORMULATION OF THE MODEL

Heat transfer at the frost surface consists of the sensible heat transfer and the latent heat transfer. The latter comes from the phase change of the water-vapor molecule. Because these phenomena are coupled, mass balance equation and energy equation should be solved in order to describe the frost growth (2005).

Frost formation is a complex process; and in order to simplify this process, the following assumptions were made.

1. Surface temperatures of the heat exchanger are under 0 ^{o}C.
2. The model is at a quasi-steady state. The numerical model was studied within a finite time interval. This situation provides possibility to a steady state system.
3. Due to the fact that heat transfer is dominant along the fin, axial heat transfer on the pipe surface is negligible.
4. The surface temperature on the tubing arrangement is regarded as variable.
5. The thermal conductivity of frost has only changed with its density.

Following the above assumptions, the governing equations for tube wall, fin, refrigerant, air and frost can be formulated.

For the solutions of the governing equations, the coil was divided into 583 control volumes as shown in Figure 1. Partial differential equations for the numerical model were solved by using the finite difference method. The Gauss-Seidel iteration method was used in solving the equations. Yang, Lee and Song in their experimental study on finned tube evaporators, obtained the following empirical formulas.

In this study, the coefficients of convection on fin side and tube side were respectively given with Eqs. (1-2) and by taking into account the coefficients of convection heat transfer on the air side (Yan et al.,2003).

$$Nu_{fin} = \frac{h_{fin} L}{k_a} = 0.204 Re_L^{0.657} Pr^{1.334} \quad (1)$$

where, h_{fin} and k_a are the convection heat transfer coefficient and thermal conductivity for the fin and air sides respectively.

$$Nu_{tube} = \frac{h_{tube} D_h}{k_a} = 0.146 Re_L^{0.917} Pr^{2.844} \quad (2)$$

where, h_{tube} and D_h respectively, indicate the coefficients of convection heat transfer on the tube side and the hydraulic diameter.

The Shah principle that has four dimensionless parameters and that can be applied to the nucleus, convectional and split areas has been defined as given below (Kakac, 1998).

$$\Psi = \frac{h_{TP}}{h_L} \quad (3)$$

where ψ is a dimensionless parameter that indicates Shah Relationship, h_{TP} and h_L are two phase heat transfer coefficient and liquid to liquid convection heat transfer coefficient respectively. N_s is a dimensionless parameter value based on Ψ as seen in Eqs. (4-7) (Kakac, 1998).

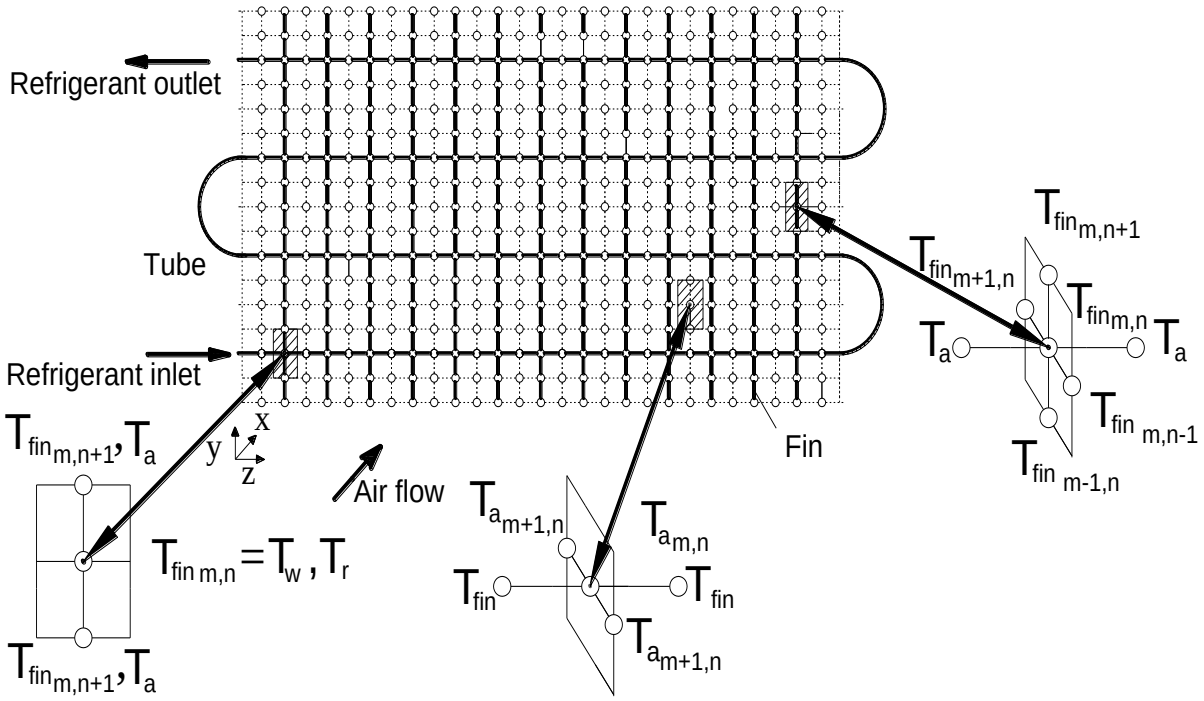

Figure 1. Division of coil for numerical solution

For Ns>1;

$$\Psi_{cb} = \frac{1.8}{N_s^{0.8}} \quad (4)$$

$$\Psi_{nb} = 230 B_0^{0.5} \qquad B_0 > 0.3\text{x}10^{-4}$$

$$\Psi_{nb} = 1 + 46 B_0^{0.5} \qquad B_0 < 0.3\text{x}10^{-4} \quad (5)$$

where B_0 is boiling number. Ψ is the highest value of Ψ_{nb} and Ψ_{cb}.

For 0.1 < Ns < 1;

$$\Psi_{bs} = F B_0^{0.5} \exp(2.74 N_s^{-0.1}) \quad (6)$$

Ψ ; is the highest value of Ψ_{bs} and Ψ_{cb}.

For $N_s \leq 0.1$;

$$\Psi_{bs} = F B_0^{0.5} \exp(2.74 N_s^{-0.15}) \quad (7)$$

Ψ ; is the largest of Ψ_{bs} and Ψ_{cb}.

According to Eqs.(6 and 7) of this study, as B_0<11x10^{-4}, then F = 15.43 (Kakac, 1998).

The thermal conductivity of frost layer depends only on the density of frost layer and is calculated with Eq. (8) (Lee rt al., 2003). (5)

$$k_{fst} = 0.132 + 3.13\text{x}10^{-4} \rho_{fst} + 1.6\text{x}10^{-7} \rho_{fst}^2 \quad (8)$$

where k_{fst} and ρ_{fst} respectively, indicate the thermal conductivity and density of frost layer. The energy equation on the tube side can be expressed as:

$$c_{p,w} . m_w \cdot \frac{\partial T_w}{\partial t} = q_t + q_{fin} - U_{a,r} A_i (T_a - T_r) \quad (9)$$

where $c_{p,w}$, m_w , q_{fin} and $U_{a,r}$ are, respectively specific heat of tube, mass of the tube, heat transferred from fin to tube and the total heat transfer coefficient from air to the refrigerant. Here q_t is the heat transfer rate from air to tube and is given by:

$$q_t = U_{a,t} A_0 (T_a - T_{tube}) \quad (10)$$

where $U_{a,t}$ shows the total heat transfer coefficient from air to tube and can be determined from

$$U_{a,t} = \frac{1}{\frac{1}{h_{tube}} + \frac{\delta_{fst}}{k_{fst}}} \quad (11)$$

The energy balance on fin side is as seen in Eq. (12)

$$m_{fin}\, c_{p,fin} \frac{\partial T_{fin}}{\partial t} = k_{fin}\, A_{tab} \frac{\partial^2 T_{fin}}{\partial x^2} w_{fin} + k_{fin}\, A_{tab} \frac{\partial^2 T_{fin}}{\partial y^2} L_{fin} + 2 A_{fin} U_{a,f} (T_a - T_{fin}) + U_m 2 A_{fin} (w_a - w_{fst}) h_{sb} \quad (12)$$

where m_{fin} and $c_{p,fin}$ are fin mass and specific heat respectively. U_m is coefficient of mass transfer and together with the coefficient of heat transfer were both calculated by using the Lewis Equation (Tso et al., 2006).

$$U_m = \frac{h_a}{Le.c_p} \quad (13)$$

where the Lewis number, Le, is taken to be 1 and 0.905 for condition without frost and frosting condition, respectively (Tso et al., 2006). $U_{a,f}$ is the total heat transfer coefficient from air to fin and is calculated by:

$$U_{a,f} = \frac{1}{\frac{1}{h_{fin}} + \frac{\delta_{fst}}{k_{fst}}} \quad (14)$$

boundary conditions for fin are set to be

$$T_{fin}(x = 0) = T_{tube}, \qquad \frac{dT_{fin}(x = w_{fin})}{dx} = 0 \quad (15)$$

$$T_{fin}(y = 0) = T_{tube}, \qquad \frac{dT_{fin}(y = L_{fin})}{dy} = 0 \quad (16)$$

By taking the inner cross section of the tube into consideration, coefficient of total heat transfer from air to refrigerant ($U_{a,r}$), can be written as

$$U_{a,r} = \frac{1}{\frac{r_i}{h_{tube}(r_o + \delta_{fst})} + \frac{r_i}{k_{fst}} In\left(\frac{r_o + \delta_{fst}}{r_o}\right) + \frac{r_i}{k_{fin}} In\left(\frac{r_o}{r_i}\right) + \frac{1}{h_r}} \quad (17)$$

The energy equation on the air side based on fin surface can be expressed as,

$$M_a.C_{p,a} \frac{\partial T_a}{\partial t} + \dot{m}_a.C_{p,a} \frac{\partial T_a}{\partial x} = h_a \cdot \frac{A_{fine}}{L_{fine}} (T_a - T_{fst}) + h_{sb}.\dot{m}_a \frac{\partial w_a}{\partial x} \quad (18)$$

where M_a, $c_{p,a}$ and h_{sb} are the air mass per unit length, specific heat of air and sublimation enthalpy of water vapor respectively. Temperature of the refrigerant is given as follows

$$M_r . c_{p.r} . \frac{\partial T_r}{\partial t} + \dot{m}_r\, h_{fg} \cdot \frac{\partial X}{\partial x} = A_i \cdot \frac{U_{a,r}}{L} (T_a - T_r) \quad (19)$$

where M_r, $c_{p,r}$ and h_{fg} are respectively, mass of the refrigerant per unit length, specific heat and latent heat of evaporation. Development of frost layer depends on the amount of water vapor transferred from the air to the frost layer.

A certain portion of the amount of water vapor transferred dissolves into frost layer and increases the frost thickness whereas another portion disperses over the porous frost layer and increases the density of the frost layer. Eq. (20) shows the total mass flow from transferred from the air to the frost layer.

$$\dot{m}''_w = U_m (w_a - w_{fst}) \quad (20)$$

where w_a and w_{fst} are absolute humidity of the atmospheric air and the air at the frost layer surface respectively. w_{fst} as seen in Eq. (21).

$$w_{fst} = \frac{0.622.P_{ws}}{P - P_{ws}} \quad (21)$$

where P_{ws} is saturation pressure on the frost layer and is given by (ASHRAE, 1997).

$$InP_{ws} = C_1/(T_{fst} + 273.15) + C_2 + C_3.(T_{fst} + 273.15) + C_4.(T_{fst} + 273.15)^2 + C_5.(T_{fst} + 273.15)^3 + C_6.(T_{fst} + 273.15)^4 + C_7.In(T_{fst} + 273.15) \quad (22)$$

where

C_1=-5674.5359
C_2=6.3925247
C_3=-0.9677843x10^{-2}
C_4=0.62215701x10^{-6}
C_5=0.20747825x10^{-8}
C_6=-0.9484024x10^{-12}
C_7=4.1635019;

Summation of the amount of water vapor ($\dot{m}''_\delta$) that increases the frost layer thickness and the amount of water vapor that increases the density of the frost layer ($\dot{m}''_\rho$) gives the total mass flow rate ($\dot{m}''_v$) transferred from humid air to the frost layer. These mass flow rates were respectively found in Eqs. (23-25).

$$\dot{m}''_v = \dot{m}''_\delta + \dot{m}''_\rho = \frac{d(\delta_{fst}\rho_{fst})}{dt} = \rho_{fst} \frac{d\delta_{fst}}{dt} + \delta_{fst} \frac{d\rho_{fst}}{dt} \quad (23)$$

$$\dot{m}''_\delta = \rho_{fst} \frac{d\delta_{fst}}{dt} \quad (24)$$

$$m''_{\rho} = \delta_{fst} \frac{d\rho_{fst}}{dt} \quad (25)$$

where δ_{fst} is frost thickness. The mass that increases frost density is given by (Tso et al., 2006)

$$m''_{\rho} = D\frac{d\rho_w}{dz} = \int_{z=0}^{z=\delta_{fst}} \varepsilon_{fst}\rho_w dz \quad (26)$$

where ε_{fst} is absorption coefficient and is defined as follow Eq. (27) (Tso et al., 2006).

$$\varepsilon_{fst} = D\left[\frac{1}{\delta_{fst}}\cosh^{-1}\left(\frac{\rho_{v,sat}(T_{fst,s})}{\rho_{v,sat}(T_{tube})}\right)\right]^2 \quad (27)$$

is coefficient of diffusion and can be expressed as below (Yao et al., 2004)

$$D = 2.302(0.98\times10^5/P_a)(T_{fst}/256)^{1.81}\times10^{-5} \quad (28)$$

ρ_v is the density of water vapor and is given by the following expression (Tso et al., 2006):

$$\rho_v(z) = \rho_{v,sat}(T_{tube})\cosh\varphi z \quad (29)$$

where φ is calculated by (Tso et al., 2006)

$$\varphi = \sqrt{\frac{\varepsilon_{fst}}{D}} \quad (30)$$

The boundary conditions for frost layer are given with Eq. (31).

at z = 0,

$$\frac{d\rho_v}{dz} = 0$$

$$\rho_v = \rho_{v,sat}(T_w) \quad (31)$$

and at $z = \delta_{fst}$, $\rho_v = \rho_{v,sat}(T_{fst,s})$

Current frost density and thickness were found by adding the increase in every step to the calculated values from the previous time interval. (Eqs.32-33)

$$\rho_{fst,t+\Delta t} = \rho_{fst,t} + \frac{m''_{\rho}}{\delta_{fst}}\Delta t \quad (32)$$

$$\delta_{fst,t+\Delta t} = \delta_{fst,t} + \frac{m''_{\delta}}{\rho_{fst}}\Delta t \quad (33)$$

The heat amount transferred into the frost layer can be given as below:

$$q''_a = m''_v h_{sb} + h_a(T_a - T_{fst}) \quad (34)$$

Eq. (35) is obtained by revising Eq.(34).

$$q_a = h_T(T_a - T_{fst})A_T \quad (35)$$

where h_T, is the convection heat transfer coefficient that represents sensible and latent heat on the air side and is written as,

$$h_T = h_a + \frac{m''_v h_{sb}}{(T_a - T_{fst})} \quad (36)$$

If Eq. (23) is taken into consideration Eq. (34) can then be written as below:

$$q''_a = \left[h_a(T_a - T_{fst}) + \rho_{fst}\frac{d\delta_{fst}}{dt}h_{sb}\right] + \delta_{fst}\frac{d\rho_{fst}}{dt}h_{sb} \quad (37)$$

The term in the brackets in Eq. (37) shows the amount of energy passed over the frost layer and can be written as follows:

$$k_{fst}\left(\frac{dT}{dz}\right)_s = h_a(T_a - T_{fst}) + \rho_{fst}\frac{d\delta_{fst}}{dt}h_{sb} \quad (38)$$

Temperature distribution on frost layer is calculated by applying the energy equation Eq. (39) to the control volume (Figure 1).

$$k_{fst}\frac{d^2T_{fst}}{dz^2} = -\varepsilon_{fst}\rho_v h_{sb} \quad (39)$$

The boundary conditions for Eq. (39) are given by:

at z=0, $T=T_{tube}$

and at $z=\delta_{fst}$, $k_{fst}\left(\frac{dT}{dz}\right)_s = q''_a$ (40)

If Eq. (39) is rearranged based on boundary conditions of Eq. (40), the temperature distribution within the frost layer is given as Eq. (41).

$$T(z) = \frac{\varepsilon_{fst}}{k_{fst}\varphi^2}h_{sb}\rho_{v,sat}(T_{tube}) (z\varphi\sinh\varphi\delta_{fst} - \cosh\varphi z + 1) + \frac{q''_a z}{k_{fst}} + T_{tube} \quad (41)$$

Fin efficiency is as in Eq. (42) (Lenic and Frankovic, 2009).

$$\eta_{fin} = \frac{\tanh(dL)}{dL} \quad (42)$$

d is written as in Eq.(43) (Lenic and Frankovic, 2009).

$$d = \sqrt{\frac{1}{\frac{\delta_{fst}}{k_{fst}} + \frac{c_{p,a}}{h_a a}} \cdot \frac{1}{k_{fin}\delta_{fin}}} \quad (43)$$

L is an equivalent fin length and has been defined as (Lenic and Frankovic, 2009)

$$L = r_o\left(\frac{r_{eq}}{r_o} - 1\right)\left(1 + 0.35.\text{In}\frac{r_{eq}}{r_o}\right) \quad (44)$$

The radius ratio $\frac{r_{eq}}{r_o}$ depends on tube row. For straight tube row, the ratio is calculated with Eq.(45) (Lenic and Frankovic, 2009).

$$\frac{r_{eq}}{r_o} = 1.28\frac{l_v}{r_o}\sqrt{\frac{l_h}{l_v} - 0.2} \quad (45)$$

As for staggered tube row, this ratio is calculated with Eq.(46) (Lenic and Frankovic, 2009).

$$\frac{r_{eq}}{r_o} = 1.27\frac{l_v}{r_o}\sqrt{\frac{l_h}{l_v} - 0.3} \quad (46)$$

Total surface efficiency is given as

$$\eta_T = 1 - \frac{A_f}{A_T}(1 - \eta_{fin}) \quad (47)$$

The overall heat transfer coefficient of the evaporator is written as

$$U = \frac{1}{\frac{1}{\eta_T h_T} + \frac{1}{h_r \frac{A_i}{A_T}} + \frac{\delta_{fst}}{k_{fst}}} \quad (48)$$

Pressure drop on air side ΔP_a is defined as (Seker et al., 2004),

$$\Delta P_a = \frac{G_{max}^2}{2\rho_i}\left[\left(1 + \sigma^2\right)\left(\frac{\rho_i}{\rho_e} - 1\right) + f_a \frac{A_T}{A_{min}}\frac{\rho_i}{\rho_m}\right] \quad (49)$$

where f_a is friction factor and can be calculated from Eq.(50) (Seker et al., 2004) as recommended by Karataş who conducted an experimental study on evaporators having same geometries.

$$f_a = 0.152\,\text{Re}^{-0.164}\,\varepsilon^{-0.331} \quad (50)$$

where ε is a scalar that shows evaporator's cooling capacity and is defined as follows (Seker et al., 2004),

$$\varepsilon = \frac{T_{ai} - T_{ao}}{T_{ai} - T_r} \quad (51)$$

EXPERIMENTAL STUDY

Schematic view of the experimental set consisting of an air tunnel, cooling system and a data logger is shown in Figure 2. Whereas diagram of the experimental set is given in Figure 3. The outer and inner diameters of the test evaporator tube placed into the air tunnel are 8 mm and 6, 72 mm respectively. The number of tubes used perpendicular to the air flow was thirteen, while that of tubes parallel to the air flow was two. In this study, an air tunnel was designed and installed in order to achieve the air conditions of the no-frost type refrigerators. Ambient air was mixed with the return air in the mixing chamber. With the help of a circulation fan, the mixture was then passed over the evaporator in the air tunnel thereby cooling it and achieving formation of frost. When the return air passes over the test evaporator the humidity decreases but it when it is mixed with the ambient air the humidity increases. In order to keep the air inlet relative humidity at a required level, a humidity absorber and a humidifier were used. With a flow straightener, the air from humidifier was sent over the evaporator. To keep the temperature at the entrance of the test evaporator at a required level a cooler and a heater were used. An interim evaporator was run until the system entered a steady state. When the system had reached steady state the refrigerant in the test evaporator was circulated. The control of the refrigerant was activated by using a solenoid valve. The refrigerant used in this study was R22 (chlorodifluoromethane).

In the experimental study, input and output air temperatures, humidity and speeds were recorded. In the measurements of refrigerant temperatures, K type thermal couples were used. A temperature-humidity meter was used to measure air temperatures and its humidity. Air velocity was recorded with an anemometer. Specifications of the measuring devices are given in Table 1. The experimental data recorded were used to calculate UA values. The experimental results obtained were compared with those of the numerical model to determine their accuracy (Holman, 1996).

RESULTS AND DISCUSSION

In this experimental study, the effects of air temperature and relative humidity on fin-tube evaporator's UA were investigated under frosting conditions. The compatibility between numerical model and experimental study is presented in Situation 1. Whereas in Situation 2, variations of UA, frost thickness and air-side pressure drop with respect to time were numerically investigated under different air conditions; and the results received from the numerical model are given too (Holman, 1996).

Situation 1:

In both the experimental study and numerical model, variations of UA versus time were investigated at different air inlet temperatures and different relative humidity. Eqs. (1-51) were used in the solution of the developed numerical model in order to determine the UA, frost thickness and pressure drop on air side. Finite Difference Method was used in solving the partial differential equations for the model. Gauss-Seidel was chosen as the iteration method in solving the equations. The T_w; T_{fin}; T_a; T_r and T_{fst} temperatures in the numerical model were found from Eqs. 9, 12, 18, 19 and

41 respectively. Numerical algorithm for the model is given in Figure 4. MATLAB R 2010 is the programming language used for the numerical model. The data for the experimental and numerical model are respectively shown in Figures 5 and 6.

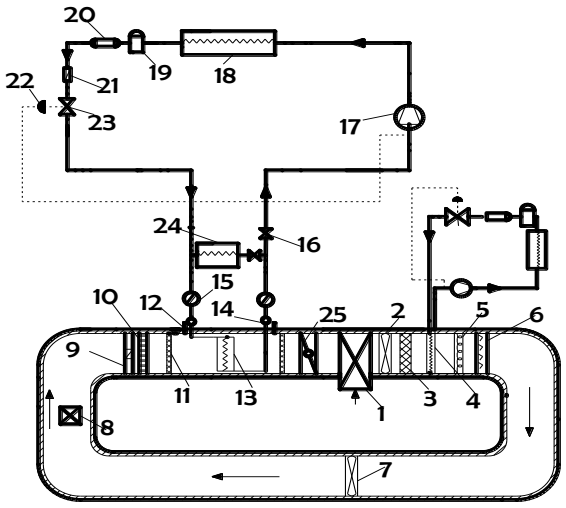

Figure 2. Schematic presentation of experimental system **Item No.** Device Name: **1.** Vent, **2.** Fan, **3.** Humidity absorber, **4.** Evaporator, **5.** Heater, **6.** Moisturizer, **7.** Fan, **8.** Vent, **9.** Damper, **10.** Flow straightener, **11.** Temperature-humidity meter, **12.** Pressure different meter, **13.** Test evaporator, **14.** Thermocouple, **15.** Manometer, **16.** Solenoid valve, **17.** Compressor, **18.** Condenser, **19.** Gas Tank, **20.** Drier, **21.** Flow meter, **22.** Valve regulator, **23.** Expansion valve, **24.** Temporary evaporator, **25.** Anemometer.

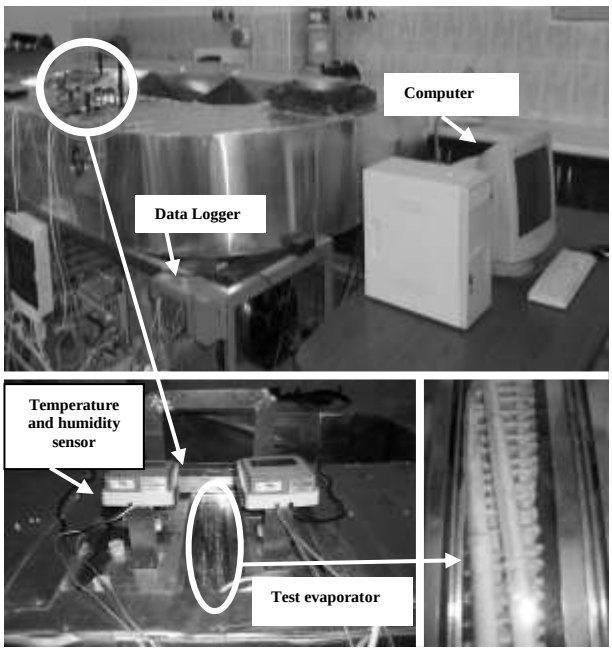

Figure 3. Picture of the experimental system

It was found that at $T_{a,i}$=9^o C the UA value is higher than at $T_{a,i}$=11^{o}C. Because the absolute humidity value at $T_{a,i}$=11^{o}C is higher than that at $T_{a,i}$=9^{o}C, the UA value at $T_{a,i}$=11^{o}C was found to be lower. Similar results were also obtained for the numerical model (Figure 5). The time leads to an enlargement of the frost thickness and hence causing the decrease in the total conductivity.

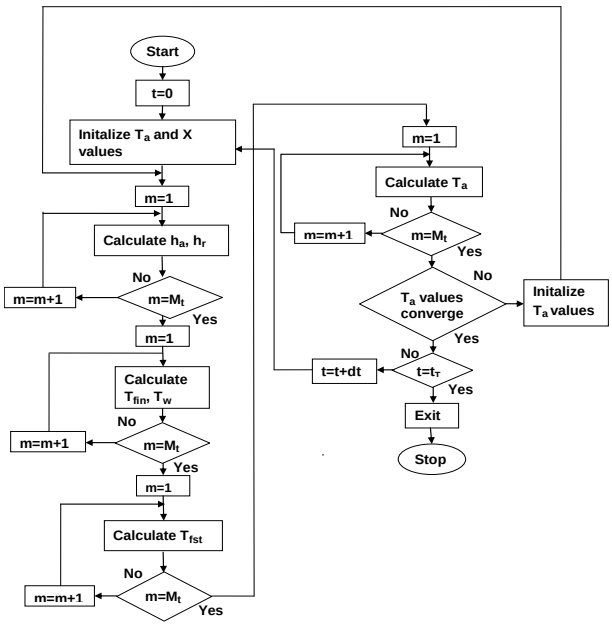

Figure 4. Algorithm of the numerical model

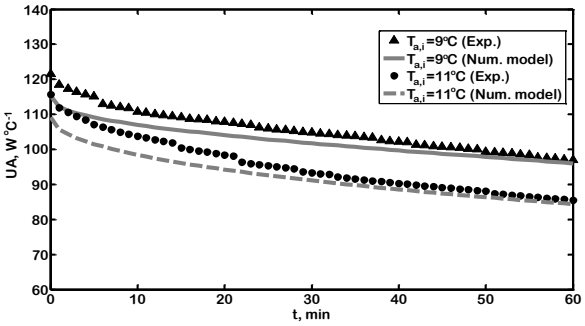

Figure 5. Variation of total conductivity with time for $T_{a,i}$=9^{o}C, Φ=65%, $u_{a,i}$=1.4 ms^{-1}; $T_{a,i}$=11^{o}C, Φ=65%, $u_{a,i}$=1.4 ms^{-1}

In Figure 6 the UA values are studied for $T_{a,i}$=7^{o}C at relative humidity rates of 55% and 75%. It was found that the UA tends to decrease as the relative humidity increases. The increase in relative humidity causes an increase in the amount of humidity in the air. The increase in humidity leads to a corresponding increase in frost thickness and this drops the UA value. It was found that the experimental results are compatible with the results obtained on the numerical model (Figure 6).

Uncertainty analysis for UA values was made with the help of Eqs. 52 and 53.

$$R = R(x_1, x_2, x_3, ..., x_n) \tag{52}$$

$$W_R = [(\frac{\partial R}{\partial x_1} W_1)^2 + (\frac{\partial R}{\partial x_2} W_2)^2 + (\frac{\partial R}{\partial x_3} W_3)^2 + ...(\frac{\partial R}{\partial x_n} W_{n1})^2]^{1/2} \tag{53}$$

where R is the value on which uncertainty analysis will be carried out, x_n represents independent variables, W_R, is the uncertainty of the required value and W_n shows the

uncertainties of independent variables (Ozen, 2011). For UA value, W_R was found to be 1.87-2.16% (Table 2).

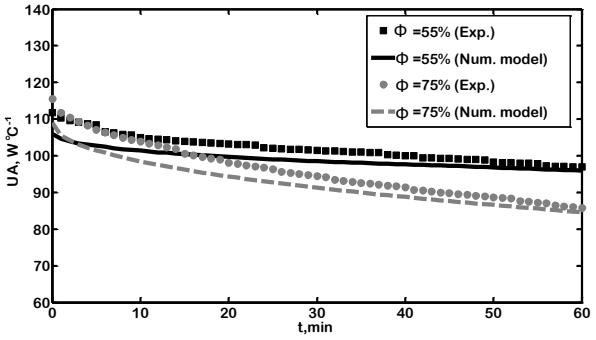

Figure 6. Variation of total conductivity with time for $T_{a,i}$=7°C, Φ=55%, $u_{a,i}$=1.3 ms^{-1}; $T_{a,i}$=7°C, Φ=75%, $u_{a,i}$=1.3 ms^{-1}

The uncertainty range using measurement accuracy for UA was estimated to be ± 2.03 %. The characteristics and uncertainties of the measurement instruments are given in Table 1.

Table 1. Characteristics and accuracies of the measurement instruments.

Instrument	Range	Accuracy
Temperature humidity meter	-20 to 80 (°C); 0-100(%R.H.)	± 1% ; ± 3.0 %
K type thermocouple	-40 to 1200 (°C)	± 1 %
Anemometer	0-15(ms^{-1})	±2%
Flow-meter	0.005 to 0.05(kg s^{-1})	±1.2 %
Pressure sensor	0 - 3000 kPa	±1.6 %

Table 2. Accuracy values for the UA

	T_a °C	Φ, %	u_a, ms^{-1}	W_{UA}, %
Exp-1	7	55	1.3	2.14
Exp-2	7	75	1.3	2.16
Exp-3	9	65	1.4	1.95
Exp-4	11	65	1.4	1.87

Situation 2:

In Situation 2, the time-based variations of UA values, frost thickness and pressure drop on the air side at different air conditions were investigated numerically and the results obtained from the numerical model are given. The effects of relative humidity, air temperature and air velocity on the total conductivity of a fin-tube evaporator, air-side pressure drop and frost thickness were numerically investigated under frosting conditions. (Figs. 7-15).

Effects of air inlet temperature on UA, frost thickness and pressure drop on air side

In order to see the effects of air temperature on the numerical model, variation of total conductivity, pressure drop and frost thickness versus time are presented in Figs. 7-9.Total conductivity increased with the drop in inlet air temperatures (Figure 7). At the same relative humidity, the humidity in the air increases with the air temperatures. The increase in the air humidity leads to an enlargement of the frost thickness and hence causing the decrease in the total conductivity. These results consistent with those obtained by Yan (4). It was observed that the total conductivity decreases with time; and this is also supported by the results obtained in the study conducted by Lenic (9). Frost thickness and pressure drop on the air side increases with temperature. The increase in pressure drop on the air side as a result of enlargement of frost thickness is an expected outcome. This outcome complies with Yan (4) (Figs. 8-9)

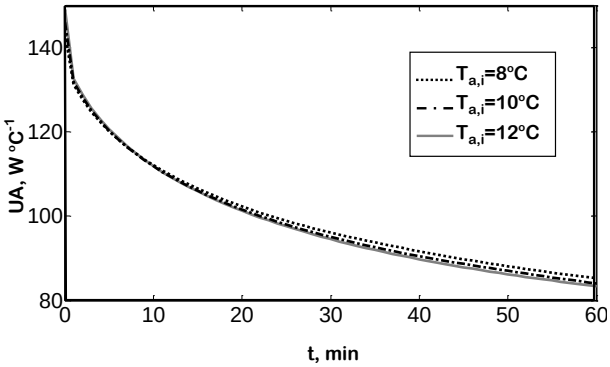

Figure 7. Variation total conductivity at different temperatures versus time under the conditions that Φ=70% and u_a =1.5 ms^{-1}

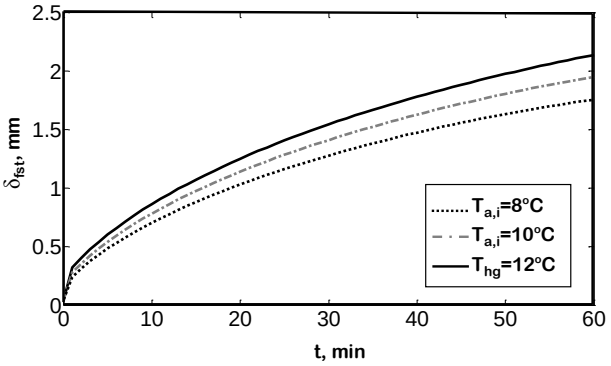

Figure 8. Variation of frost thickness with time under variable temperatures for Φ=70%, and u_a =1.5 ms^{-1}

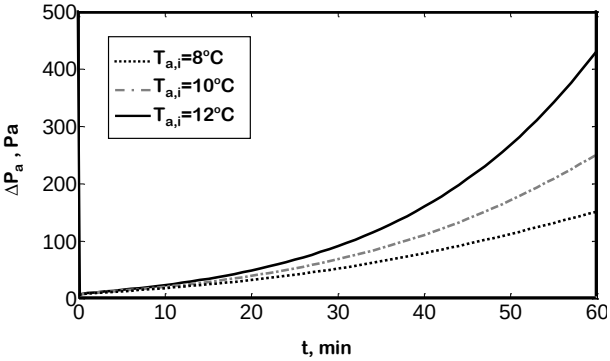

Figure 9. Variation of air side pressure drop with time under variable temperatures for Φ=70%, and u_a =1.5 ms^{-1}

Effects of relative humidity on UA, frost thickness and pressure drop on air side

Time-based variations of UA, frost thickness and pressure drop on the air side for relative humidity rates of 60%, 70% and 80% are given in the numerical model are presented on Figs. 10-12. As seen in Figure 10, as

the relative humidity increases, the total conductivity decreases. This result resembles those obtained by Yan (4), Kondepudi and O'Neal (1). The increase in relative humidity leads to an increase in the air humidity and consequently resulting in the thickening of the frost layer (Figure 11). The enlarged frost layer narrows the cross section area through which the air passes. The decrease in cross section area leads to a corresponding increase in the pressure drop on the air side (Figure 12). These results are similar to those obtained by Seker (6), Yan (4) and Kondepudi et al (1).

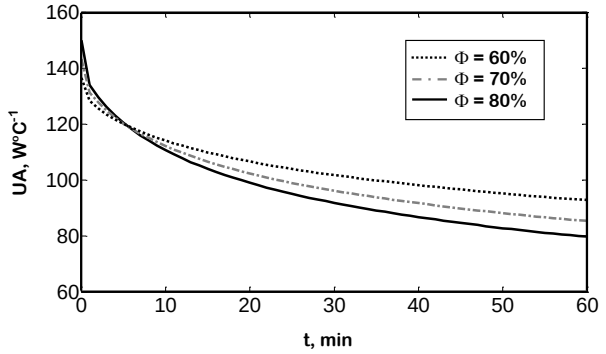

Figure 10. Variation of total conductivity with time at Ta_{in}=8°C,$u_{a,i}$=1.5 ms^{-1} for different relative humidity

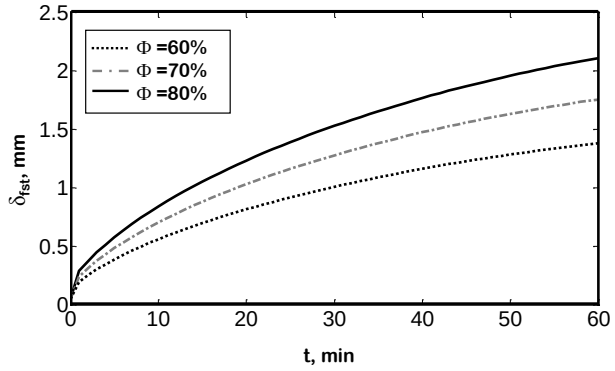

Figure 11. Variation of frost thickness with time at $T_{a,i}$=8°C,$u_{a,i}$=1.5 ms^{-1} for different relative humidity values

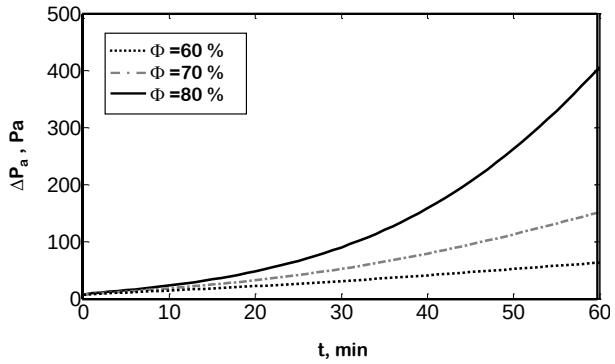

Figure 12. Variation of air side pressure drop with time at $T_{a,i}$=8°C and $u_{a,i}$=1.5 ms^{-1} for different relative humidity

Effects of air velocity on UA, frost thickness and pressure drop on air side

In order to observe the effects of air velocity on UA, frost thickness and pressure drop on the air side, three different air velocities ($u_{a,i}$=0.7, 1, 1.3 m s^{-1}) were numerically investigated (Figs.13-15). It was found in this study that, as the air velocity increases, total conductivity and pressure drop increase too (Figs.13-15). These are also the results obtained by Seker (6) and Yan (4). It was concluded that the effects of changes of air velocity on frost thickness can be neglected (Figure 14). These results consistent with those obtained by Hermes (7).

Comparisons of the results obtained from this study with those from the other studies in the literature are given in Tables 3-5. The (+) and (-) in Tables 3-5 respectively indicate increase and decrease in UA, δ_{fst} and ΔP_a values, whereas (0) shows that no change, whatsoever, exists in UA, δ_{fst} and ΔP_a. Meanwhile (…) indicates that the authors have no referenced studies on the topic.

Table3. Effects of increasing air temperature on UA, δ_{fst} and ΔPa

Authors	UA, W K^{-1}	δ_{fst}, m
Seker et al.(6)	+	+
Yan et al. (4)	+	…
Present study	+	0

Table 4. Effects of increasing relative humidity on UA, δ_{fst} and ΔP**a**

Authors	UA, W K^{-1}	δ_{fst}, m
Seker et al.(6)	+	+
Yan et al. (4)	-	…
Present study	-	+

Table 5. Effects of increasing air velocity on UA, δ_{fst} and ΔP**a**

Authors	UA, W K^{-1}	δ_{fst}, m
Seker et al.(6)	+	+
Yan et al. (4)	-	…
Present study	-	+

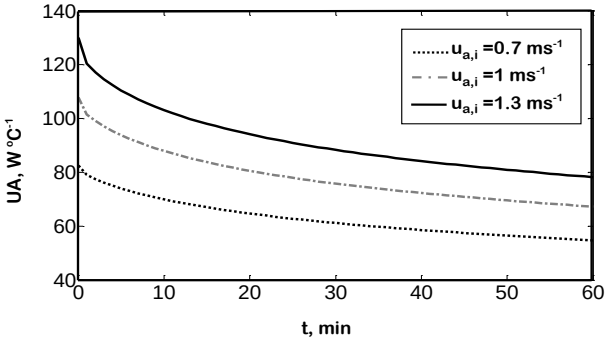

Figure 13. Variation of total conductivity with time at $T_{a,i}$ =8°C, Φ=70% for different air velocities

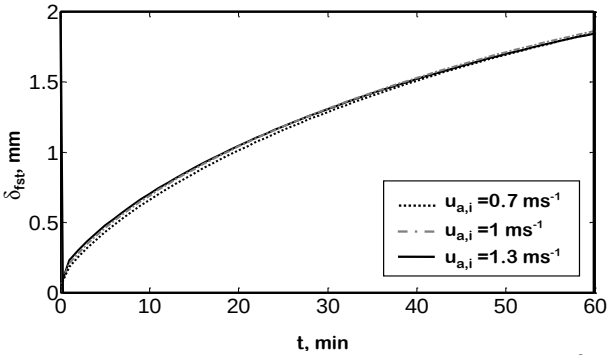

Figure 14. Variation of frost thickness with time at $T_{a,i}$=8 °C, Φ=70% for different air velocities

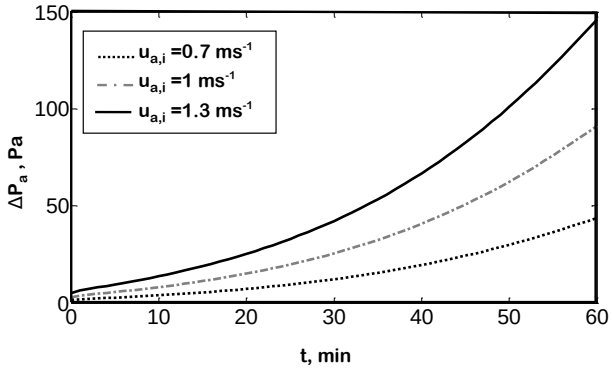

Figure 15. Variation of air side pressure drop with time at $T_{a,i}$=8 ^{o}C, Φ=70% for different air velocities

CONCLUSION

In this study, performance of a fin-tube evaporator under frosting conditions was investigated both experimentally and numerically, and the results presented as follows:

- As the air temperature increases, frost layer and pressure drop on the air side increase also while total conductivity decreases. (Figs.7-9).
- Total conductivity decreases with an increase in relative humidity. The frost layer and the air-side pressure drop increase (Figs.10-12).
- With this study, it was found that air velocity has negligible effects on frost thickness (Figure 14).

The experimental results are compatible with the results obtained on the numerical model. When the experimental results are compared with those obtained from the numerical model, it is found that they both give almost the same overall conductivity (%3.08-%7.24) of the evaporator. Consequently, with this study it has been shown that the frost model presented in this study can be applied in other similar studies as well.

ACKNOWLEDGMENT

Financial support of this study by the research fund of the Selcuk University under Grant No. BAP 09101048 is gratefully acknowledged.

REFERENCES

ASHRAE Handbook of Fundamentals, 1997.

Getu H.M., Bansal P.K. , 2011, New frost property correlations for a flat-finned-tube heat exchanger, *International Journal of Thermal Sciences*, 50, 544–557.

Hermes C.J.L. , Piucco R. O., Barbosa J.R., Melo C., 2009, A study of frost growth and densification on flat surfaces, *Experimental Thermal and Fluid Science* 33, 371-379.

Holman, J.P., Experimental Methods for Engineers, McGraw-Hill, Kogakusha,1966.

Kakac, S., 1998. Soğutma ve Havalandırma Sistemleri için Evaporatörler ve Yoğuşturucular ve Isı Tasarımları, *The 3rd International Symposium for Installation Science and Technology in Structures*.

Kondepudi S.N., O'Neal D.L., 1989, Effect of frost growth on the performance of louvered finned tube heat exchangers, *Int. J. Refrig*. 12, 151-158.

Kondepudi S.N., O'Neal D.L., 1993, Performance of finned-tube heat exchanger under frosting conditions: I. Simulation model, *Int. J.Refrigeration* 16, 175-180.

Kondepudi S.N., O'Neal D.L., 1993, Performance of finned-tube heat exchanger under frosting conditions: II. Comparison of experimentaldata with model, *Int. J. Refrigeration*, 16, 181-184.

Lee Y.B. , Ro S.T. , 2005, Analysis of the frost growth on a flat plate by simple models of saturation and supersaturation, *Experimental Thermal and Fluid Science*, 29, 685–696.

Lee K.S. , Jhee S. , Yang D.K., 2003, Prediction of the frost formation on a cold flat surface, *International Journal of Heat and Mass Transfer*, 46, 3789-3796.

Lenic K., Trp A., Frankovic B., 2009, Prediction of an effective cooling output of the fin-and-tube heat exchanger under frosting conditions, *Applied Thermal Engineering*, 29, 2534-2543.

Moallem E., Hong T., Cremaschi L., Fisher D.E., Experimental investigation of adverse effect of frost formation on microchannel evaporators, part 1: Effect of fin geometry and environmental effects, *International Journal of Refrigeration*, In Press, Corrected Proof, Available online 23 September 2012

Ozen, D.N, 2011, Investıgated Of Performance Of Fınned Tube Evaporators Under Frostıng Conditions, Selcuk University Ph.D Thesis, Turkey.

Seker D., Karatas H., Egrican Nilufer, 2004, Frost formation on fin-and-tube heat exchangers. Part I-Modeling of frost formation on fin-and-tube heat exchangers, *International Journal of Refrigeration*, 27, 367-374.

Seker D., Karatas H., Egrican Nilufer, 2004, Frost formation on fin- and- tube heat exchangers. Part II-Experimental investigation of frost formation on fin-and- tube heat exchangers, *International Journal of Refrigeration* 27, 375-377.

Tso C.P., Cheng Y.C., Lai A.C.K., 2006, An improved model for predicting performance of finned tube heat exchanger under frosting condition, with frost thickness variation along fin, *Applied Thermal Engineering*, 26, 111-120.

Wang W., Guo Q.C., Feng Y.C., Lu W.P., Dong X.G., Zhu J.H., 2013, Theoretical study on the critical heat and mass transfer characteristics of a frosting tube. *Applied Thermal Engineering*, 54, 153-160.

Yan W.M., Li H. Y., Wu Y. J., Lin J.Y., Chang W. R, 2003, Performance of finned tube heat exchangers operating under frosting conditions, *International Journal of Heat and Mass Transfer*, 46, 871-877.

Yao Y., Jiang Y., Deng S. , Ma Z., 2004, A study on the performance of the airside heat exchanger under frosting in an air source heat pump water heater/chiller unit, *International Journal of Heat and Mass Transfer* 47, 3745-3756.